Sufficient field-of-view for the M-line method in cone-beam CT

Nicolas Gindrier, Rolf Clackdoyle, Simon Rit, Laurent Desbat

Sufficient Field of View for the M-line Method in Cone-beam CT

Nicolas Gindrier, Rolf Clackdoyle, Simon Rit and Laurent Desbat

***Abstract*—This work concerns region-of-interest reconstruction in cone-beam CT with transverse and axial truncation. We study two cylindrical fields of view configurations with a saddle X-ray source trajectory. We give sufficient conditions for accurate image reconstruction with the M-line method.**

I. Introduction

In cone beam CT, Tuy [1] and Finch [2] proved that exact reconstruction is only possible within the convex hull of a source trajectory S (provided S is connected and bounded, as is usually the case), as long as the cone-beam projections are not truncated. Truncation arises when the measured X-ray cone beam does not cover the whole object transversely and/or axially (Fig. 3). For a helical trajectory of the x-ray source, Zou and Pan [3] showed that some truncation can be handled with the differentiated backprojection (DBP) method and their approach directly applies to certain other source trajectories. This method can be coupled with the M-line method [4] for more flexibility in handling truncation.

In this work, we assume that the object support is contained in a cylindrical region called Ω_o and we address the case of simultaneous transverse and axial truncation. We study the saddle trajectory, defined by $S = \{(R\cos\lambda, R\sin\lambda, H\sin(2\lambda)), \lambda \in [0, 2\pi)\}$, where $R > 0, H > 0$. The saddle trajectory is connected, bounded and closed, see Fig. 3. It is known that the union of all its chords (line segments that connect two points on trajectory) is the same as the convex hull C_S of the trajectory (Fig. 1)[5], so anything outside this region cannot be reliably reconstructed. However, feasibility of reconstruction inside the region will depend on the pattern of truncation of the projections. For the saddle trajectory, [5] and [6] only deal with axial truncation whereas [7] only focuses on transverse truncation.

Each x-ray source generates a (solid) cone of line segments determined by a corresponding detector. The FOV is defined here as the intersection of all measured X-ray cones from all source positions, as illustrated in Fig. 2. Note that for the same trajectory, different patterns of truncation (different detector geometries) will generate different FOVs. We say that a FOV is *sufficient* if, relative to the (known) object support, certain conditions to ensure an exact reconstruction are met.

Specifically, we assume that both Ω_o and the FOV are cylinders whose axes are parallel to the $\boldsymbol{x}_3$-axis, see Fig. 3 (however, in practice, it is difficult to build a FOV with a perfect cylindrical shape). Neither of these regions are necessarily contained with C_S, the region of potentially feasible reconstruction.

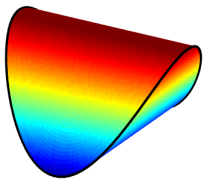

Fig. 1. The convex hull C_S of the saddle trajectory. Each point of this convex set is intersected by a chord.

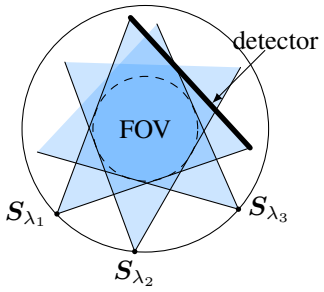

Fig. 2. The FOV defined as the intersection of the X-ray cones (here we show a 2D version, with three source positions). With the saddle trajectory, it is impossible to perfectly define a cylindrical FOV using a rectangular detector, but for simplicity we investigate a cylinder inside this FOV.

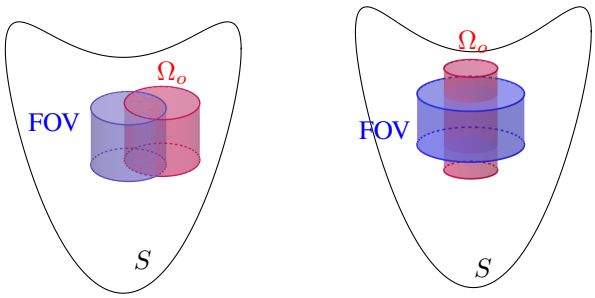

Fig. 3. The saddle trajectory S with a cylindrical FOV and Ω_o containing the object support. *Left*: Transverse truncation. *Right*: Axial truncation.

The DBP method allows a point $\boldsymbol{x} \in \text{FOV} \cap C_S \cap \Omega_o$ to be reconstructed if it lies on a chord (a line linking two source

Manuscript received December 21, 2020. This work was supported by the "Fonds unique interministériel" (FUI) and the European Union FEDER in Auvergne Rhône Alpes (3D4Carm project) and by the ANR (ROIdoré project ANR-17-CE19-0006-01).

N. Gindrier, R. Clackdoyle and L. Desbat are with the TIMC-IMAG laboratory, CNRS UMR 5525 and Univ. Grenoble Alpes 38000 Grenoble, France. e-mail: nicolas.gindrier@univ-grenoble-alpes.fr

S. Rit is with Univ. Lyon, INSA-Lyon, UCB Lyon 1, UJM-Saint Etienne, CNRS, Inserm, CREATIS UMR5220, U1206, Centre Léon Bérard, F-69373, LYON, France.

978-1-7281-7693-2/20/$31.00 ©2020 IEEE

positions of the trajectory, see Fig. 4) and if the intersection of the chord and the FOV contains a non empty interval outside the object Ω_o, see [8], [9], [4], [10]. This geometrical requirement is generated by requirements for a subsequent inversion step using the one-endpoint Hilbert transform [10], but we do not concern ourselves here with those details. When the second condition fails, it might be possible to resort to the M-line method. An M-line is a half-line from a source position and passing through $\boldsymbol{x}$ (see Fig. 4). To reconstruct $\boldsymbol{x}$, the intersection between the FOV and the M-line passing through $\boldsymbol{x}$ must contain an interval outside the object Ω_o: the M-line must intersect the region $\Omega_F = \mathrm{FOV} \setminus \Omega_o$. There can be many possible M-line configurations satisfying this condition (see Fig. 5). Moreover, each point on the interval of the M-line that intersects $\mathrm{FOV} \cap \Omega_o$ must lie on a chord (a different chord for each such point). As $\boldsymbol{x}$ is in the convex-hull of S, an M-line segment from a source-point to $\boldsymbol{x}$ is also in this convex hull, therefore each point on this segment lies on its own chord. In [7], cone-beam reconstruction using the M-line trajectory was presented for the saddle trajectory with transverse truncation.

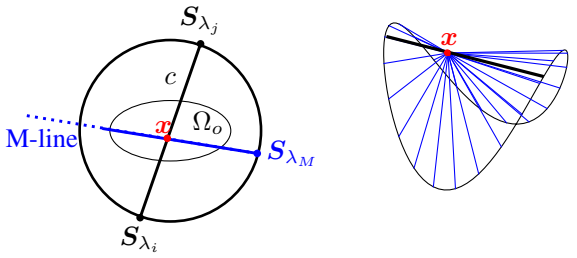

Fig. 4. *Left:* Top view of a chord c and an M-line from S_{λ_M}. *Right:* Parts of some M-lines (in blue) through a point $\boldsymbol{x}$ which is inside the convex hull C_S of the saddle trajectory. A chord (in black) contains $\boldsymbol{x}$.

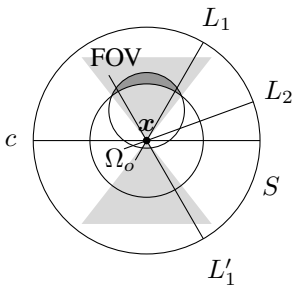

Fig. 5. Top view of a saddle trajectory S and an object with support Ω_o. Here, $\boldsymbol{x}$ is on the chord c and the DBP method cannot be directly applied, because $c \cap \mathrm{FOV}$ is in the strict interior of $c \cap \Omega_o$, see [10]. However, M-line method can be applied here. L_1 is a suitable M-line, because $L_1 \cap \Omega_F \neq \emptyset$ ($\Omega_F = \mathrm{FOV} \setminus \Omega_o$ is the dark grey region). Similarly for L_1' but not for L_2 (see [10] and [4]). The grey cones delimit the suitable M-lines.

When both transverse and axial truncation are present, correct application of the M-line method requires careful examination of the geometry of the FOV and the object Ω_O. Fig. 6 gives an example of an unsuitable FOV for the saddle trajectory S because, for the chosen $\boldsymbol{x}$, there is no M-line crossing Ω_F. An M-line is suitable only if its intersection with Ω_F contains an interval of finite length.

Our aim is to define FOVs such that each point of the region of interest (ROI) $\Omega_o \cap \mathrm{FOV} \cap C_S$ can be reconstructed with

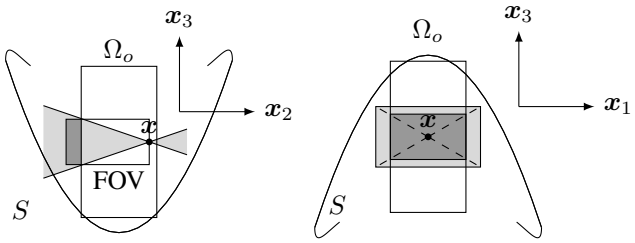

Fig. 6. An example FOV not suitable for the M-line method, because the (two) cones of lines (light grey) from $\boldsymbol{x}$ which intersect $\mathrm{FOV} \setminus \Omega_o$ (dark grey) do not intersect the saddle trajectory S. Therefore there can be no M-line that intersects $\mathrm{FOV} \setminus \Omega_o$, and reconstruction inside all $\mathrm{FOV} \cap \Omega_o$ cannot be performed using the M-line method.

the M-line method, assuming $\Omega_F \neq \emptyset$. We call these FOVs *sufficient* FOVs.

In this work, we focus on two sufficient FOV configurations mixing transverse and axial truncation. They will be called *type 1* and *type 2*.

II. Sufficient Fields of View

We begin by considering the case of axial truncation only (i.e., in projection on the horizontal plane $(\boldsymbol{x}_1, \boldsymbol{x}_2)$, the object is contained in the FOV, as illustrated in Fig. 3, right). For simplicity, we assume that the cylinders FOV and Ω_o share the same axis. Let $\boldsymbol{x} \in \Omega_o \cap \mathrm{FOV} \cap C_S$, then the intersection between Ω_F and a horizontal plane containing $\boldsymbol{x}$ is an annulus. Now $\boldsymbol{x}$ is in C_S, the convex hull of S, so we denote one of these intersections with the horizontal plane by $\boldsymbol{S}_\lambda$. See Fig. 7 for an illustration. Then, an M-line from $\boldsymbol{S}_\lambda$ and passing through $\boldsymbol{x}$ intersects the annulus previously mentioned, so this M-line is suitable and the FOV is sufficient. By convexity, the segment connecting $\boldsymbol{S}_\lambda$ to $\boldsymbol{x}$ is inside C_S, therefore each point of this segment lies on some chord, as required in order for the M-line to be suitable. The case of saddle trajectory with only axial truncation was treated in [5] and [6], but with other methods than the DBP method.

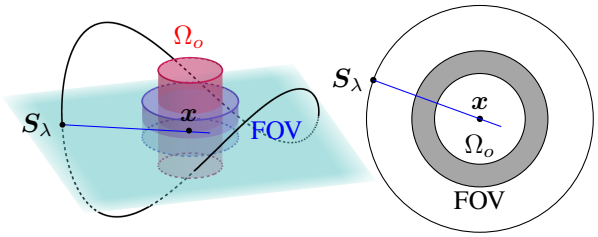

Fig. 7. A saddle trajectory with only axial truncation. Considering a horizontal plane through $\boldsymbol{x} \in \Omega_o \cap C_S \cap FOV$, it is possible to have a suitable M-line (in blue) from an intersection between the horizontal plane and the trajectory. *Right*: top view, the dark grey annulus is Ω_F.

From now on, we will work with another configuration with transverse truncation, with in addition sometimes axial truncation (an example is given Fig. 8). In this case, the projections of Ω_o and the FOV onto the horizontal plane $(\boldsymbol{x}_1, \boldsymbol{x}_2)$ intersect, such as shown in Fig. 5 i.e., if D_o (resp. D_{FOV}) is the disk defined by the orthogonal projection of the cylinder Ω_o (resp. FOV) onto the plane $(\boldsymbol{x}_1, \boldsymbol{x}_2)$, then we assume $D_{\mathrm{FOV}} \cap D_o \neq \emptyset$.

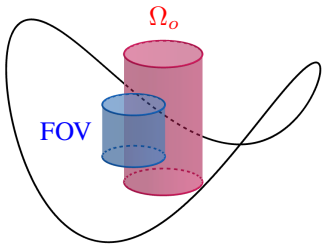

Fig. 8. A saddle trajectory with axial and transverse truncation.

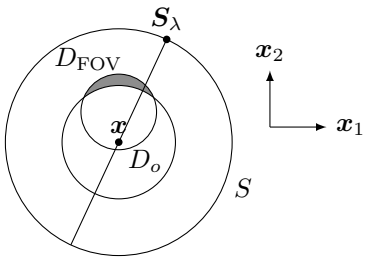

Fig. 10. Projected view from above (onto the horizontal plane $(\boldsymbol{x}_1, \boldsymbol{x}_2)$) showing a vertical plane containing $\boldsymbol{x}$ passing through $D_{\mathrm{FOV}} \setminus D_o$ (in dark grey). It intersects the saddle trajectory S in two points, and $\boldsymbol{S}_\lambda$ is the point such as the projection of $[\boldsymbol{x}, \boldsymbol{S}_\lambda]$ intersects $D_{\mathrm{FOV}} \setminus D_o$.

We now give conditions for a FOV to be sufficient, thus ensuring the ROI can be reconstructed using the M-line method.

a) Sufficient FOV: type 1: For each extremity of the cylindrical FOV (the base or the cap), one of the two following conditions must be satisfied:

- the extremity is outside C_S.
- the extremity is beyond the object (the FOV has a non empty intersection with the corresponding extreme base (or cap) of Ω_o).

Such a FOV is called *sufficient of type 1*.

The sufficiency of a type 1 FOV can be justified by considering any vertical plane (i.e. parallel to the $\boldsymbol{x}_3$-axis) containing a point $\boldsymbol{x}$ of the ROI and intersecting Ω_F (see Fig. 9), or equivalently in orthogonal projection onto $(\boldsymbol{x}_1, \boldsymbol{x}_2)$, intersecting $D_{\mathrm{FOV}} \setminus D_o$ (see Fig. 10).

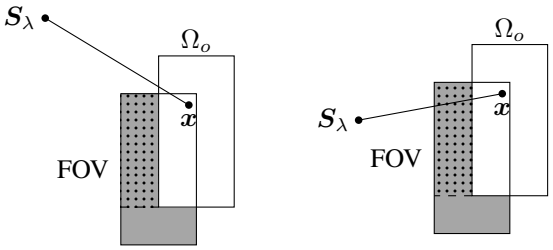

Fig. 9. Side view and cross section for a cylindrical object and a cylindrical FOV. The dark grey part is Ω_F. The horizontal plane of Fig. 10 will pass through the dotted region because $\boldsymbol{x} \in \mathrm{FOV} \cap \Omega_o$. *Left:* A potential but unsuitable M-line from $\boldsymbol{x}$ to $\boldsymbol{S}_\lambda$ is shown. This case must be avoided. *Right:* A potential and suitable M-line from $\boldsymbol{x}$ to $\boldsymbol{S}_\lambda$ is shown.

The point $\boldsymbol{x}$ being in C_S, this vertical plane will intersect the trajectory at two points. Let $\boldsymbol{S}_\lambda$ such that the projection of the segment $[\boldsymbol{x}, \boldsymbol{S}_\lambda]$ in the $(\boldsymbol{x}_1, \boldsymbol{x}_2)$ plane intersects $D_{\mathrm{FOV}} \setminus D_o$ (see Fig. 10).

We consider the $[\boldsymbol{x}, \boldsymbol{S}_\lambda]$ line segment. We must verify that this segment of M-line intersects Ω_F (with non-zero length), i.e. that the situation of Fig. 9 does not occur. For the case where both extremities of the FOV are beyond Ω_o, then $[\boldsymbol{x}, \boldsymbol{S}_\lambda]$ clearly intersects Ω_F. In the case where both extremities of the FOV are outside C_S, we first recall that, by convexity, the segment $[\boldsymbol{x}, \boldsymbol{S}_\lambda]$ is always contained in C_S (because their endpoints are). Since the extremities of the FOV are outside C_S, the segment $[\boldsymbol{x}, \boldsymbol{S}_\lambda]$ must intersect Ω_F. The remaining case (one end outside C_S and one outside the object Ω_o) is a mixture of the previous cases, and then $[\boldsymbol{x}, \boldsymbol{S}_\lambda]$ intersects Ω_F again. This last case is illustrated Fig. 11. Another way to understand conditions for FOV of type 1 is to consider two cases, in assuming these conditions are satisfied:

- The $[\boldsymbol{x}, \boldsymbol{S}_\lambda]$ line segment intersects an extremity of the cylindrical FOV: $[\boldsymbol{x}, \boldsymbol{S}_\lambda] \in C_S$, thus the satisfied condition for this case cannot be "the extremity of the FOV is outside C_S", therefore the satisfied condition is "the extremity of the FOV is beyond Ω_o", so $[\boldsymbol{x}, \boldsymbol{S}_\lambda]$ intersects Ω_F.
- The $[\boldsymbol{x}, \boldsymbol{S}_\lambda]$ line segment intersects the side of the cylindrical FOV: in this case both conditions can be satisfied, and in each case it guarantees that $[\boldsymbol{x}, \boldsymbol{S}_\lambda]$ intersects Ω_F.

We have shown that an M-line coming from $\boldsymbol{S}_\lambda$ and passing through $\boldsymbol{x}$ (and thus containing $[\boldsymbol{x}, \boldsymbol{S}_\lambda]$) intersects Ω_F and is therefore suitable, recalling that $[\boldsymbol{x}, \boldsymbol{S}_\lambda] \in C_S$ means that every point on this M-line segment lies on some chord.

Sufficient FOVs of type 1 are well suited for transverse truncation, because the constraint mainly concerns the height of the FOV.

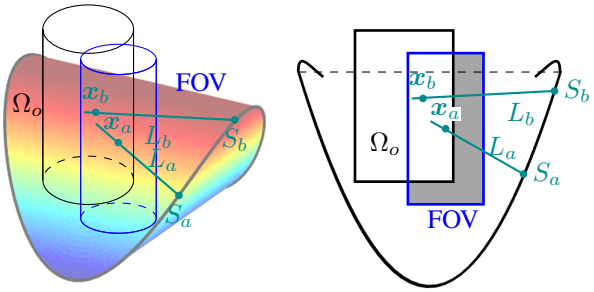

Fig. 11. An example of sufficient FOV of type 1, because the top extremity of the FOV is above C_S and the bottom extremity is below Ω_o. L_a and L_b are suitable M-lines from S_a and S_b and can be used to reconstruct $\boldsymbol{x}_a$ and $\boldsymbol{x}_b$. *Right:* Ω_F is the dark grey region.

b) Sufficient FOV: type 2: For a slice parallel to the $(\boldsymbol{x}_1, \boldsymbol{x}_2)$ plane, we denote by F_1 and F_2 the intersection points of the boundaries of Ω_o and the FOV, as in Fig. 12. A FOV is called *semicircular* if $[F_1, F_2]$ is on or below the FOV center, in the configuration of Fig. 12 (left). We consider a *semicircular* FOV and the orthogonal projection of this FOV onto a plane parallel to the vertical plane (parallel to $\boldsymbol{x}_3$) containing F_1 and F_2. If the orthogonal projection of S onto this plane intersects the orthogonal projection of the FOV, then there is

a suitable M-line for all points in the ROI and the ROI can be reconstructed. A semicircular FOV that satisfies this orthogonal projection criterion is called *sufficient of type 2* (see Fig. 12). Sufficient FOVs of type 2 are well suited for axial truncation.

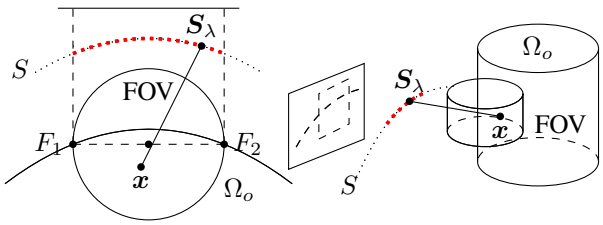

Fig. 12. Top view (*left*) and side view (*right*) for a semicircular FOV with an M-line from $\boldsymbol{S}_\lambda$ and passing through $\boldsymbol{x}$. The red dotted curve is the part of the source trajectory S whose projection intersects the projection of the FOV. For each point $\boldsymbol{x}$ of $\Omega_o \cap FOV \cap C_S$, every M-line from a source position $\boldsymbol{S}_\lambda$ from the red part of the source trajectory S is suitable. *Right*: the dashed rectangle is the projection of the FOV onto a plane parallel to the vertical plane containing F_1 and F_2. The dashed curve is the projection of the trajectory S.

III. Simulations

We simulated cone beam projections of the Forbild thorax phantom with a saddle trajectory ($R = 250$ mm and $H = 100$ mm) for three different FOVs (Fig. 13). Unlike to what Fig. 13 might suggest, for the $\boldsymbol{x}_2$-coordinate, the FOV is in fact centered on the center of rotation and the Forbild thorax phantom is off center. Nevertheless, for visualization purposes, we pretend that the fantom is fixed. We did not use the M-line method but algebraic reconstruction with the conjugate gradient method to evaluate the reconstruction quality. FOV1 is not sufficient; FOV2 is *sufficient of type 1*; FOV3 is *sufficient of type 2*. FOV1 and FOV2 are almost interior problems. In the following table (the unit is mm), R_F and H_F are respectively the radius and the height of the cylindrical FOV, C_F is the center of its base and dim_det is the dimensions of the detector (number of lines and columns); the pixel size is 2 mm $\times$ 2 mm. We analytically simulated 200 projections. CT images were reconstructed with $380 \times 152 \times 382$ voxels. Finally, we fixed $\gamma = 100$ for the conjugate gradient method from RTK [11] (minimizes $\|(Rf - p)\|_2^2 + \gamma\|\nabla f\|_2^2$ with R the forward projection operator and p the measured projections).

FOV	R_F	H_F	C_F	sufficient	dim_det
1		18	(0,30,78)	not	92×69
2	50	380	(0,30,-190)	type 1	92×437
3		18	(0,67,78)	type 2	92×69

Fig. 14 shows cross-sections at $x_3 = 84$ mm for the reconstructed images for the three FOVs, and Fig. 15 shows corresponding line profiles at $x_2 = 37$ mm. All FOVs yield good reconstructions, probably because *sufficient* FOVs correspond to sufficient but not necessary conditions. However, the convergence for FOV1 was slower: at 40 iterations, we observe a global shift of the pixel intensity values.

IV. Conclusion

In the context of cone-beam CT with a saddle trajectory and truncation, we have presented two types of *sufficient* FOVs, corresponding to two sufficient geometric conditions for accurate reconstruction of the ROI, defined as $\mathrm{FOV} \cap C_S \cap \Omega_o$. The conditions of type 1 are well suited to transverse truncation whereas the conditions of type 2 are well suited to axial truncation (there is also transverse truncation, but constraints are stronger than for type 1). It is interesting to note that fairly large truncation can be accommodated, even with an exact reconstruction. This is encouraging for reconstructing projections obtained with small detectors. However, the FOV must always be at the edge of the object support to avoid the interior problem.

Note that the proposed conditions are sufficient but not necessary. FOVs that do not meet the sufficient conditions presented in this work might still admit perfect reconstructions even though no verifying theory currently exists; apparently FOV1 is an example of such a case. For FOV1, there is probably less data redundancy and information. It may be the reason why the reconstruction of such FOVs converges but is slower than with sufficient FOVs.

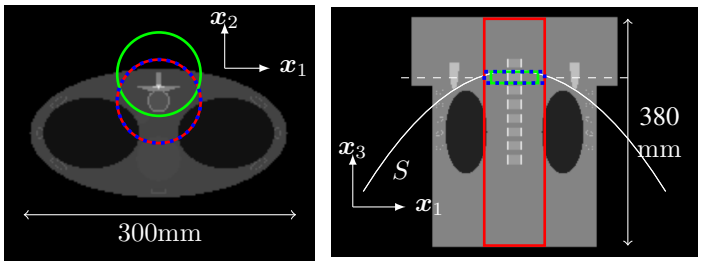

Fig. 13. Forbild thorax phantom in top view (*left*) and side view (*right*). FOV1 is represented by the blue dotted line, FOV2 is the red line and FOV3 is the green line. The white dashed line in the image at right corresponds to the profiles plot in Fig. 15. It can be seen on the right image that the projection (of the top) of FOV3 on a plane orthogonal to $\boldsymbol{x}_2$ intersects the projection of S, thus making it type 2 sufficient.

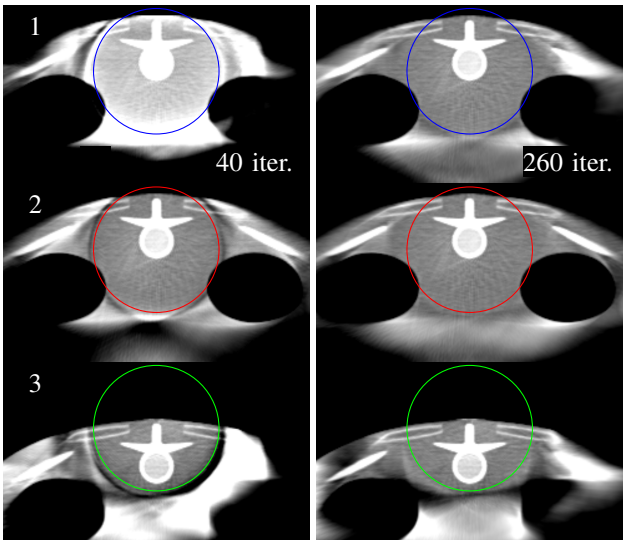

Fig. 14. Reconstructions at $x_3 = 84$ mm. *Left*: 40 iterations. *Right*: 260 iterations, for FOV1 (top), FOV2 (middle), FOV3 (bottom). The circles show the FOVs.

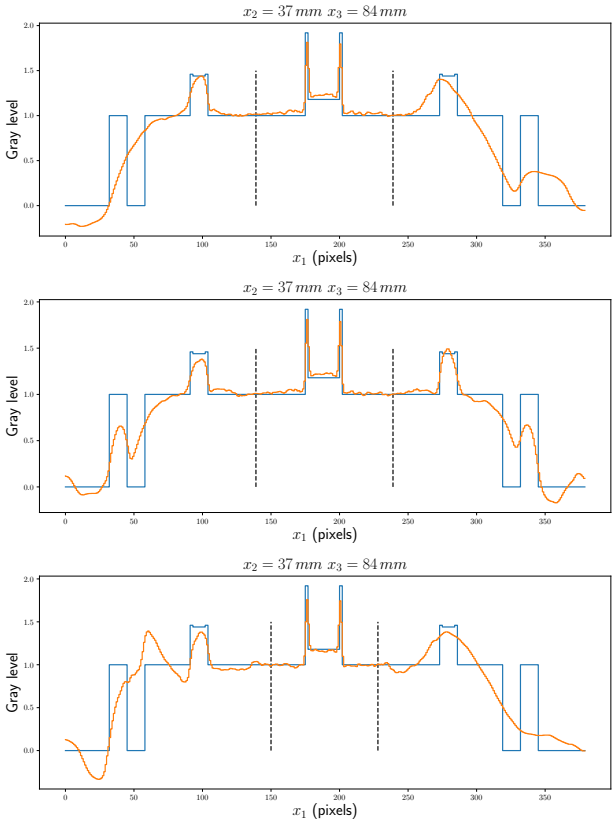

Fig. 15. Profiles (phantom in blue, reconstruction in orange) from the reconstructions after 260 iterations at $\boldsymbol{x}_2 = 37$ mm and $\boldsymbol{x}_3 = 84$ mm (see Fig. 13 *right*) for FOV1 (top), FOV2 (middle), FOV3 (bottom). The black dashed lines define the limits of the FOV.

REFERENCES

[1] H. K. Tuy, "Inversion Formula For Cone-Beam Reconstruction," *SIAM Journal on Applied Mathematics*, vol. 43, no. 3, pp. 546–552, 1983.

[2] D. V. Finch, "Cone Beam Reconstruction with Sources on a Curve," *SIAM Journal on Applied Mathematics*, vol. 45, no. 4, pp. 665–673, 1985.

[3] Y. Zou and X. Pan, "Exact image reconstruction on PI-lines from minimum data in helical cone-beam CT," *Physics in Medicine and Biology*, vol. 49, no. 6, pp. 941–959, 2004.

[4] J. D. Pack, F. Noo, and R. Clackdoyle, "Cone-beam reconstruction using the backprojection of locally filtered projections," *IEEE Transactions on Medical Imaging*, vol. 24, no. 1, pp. 70–85, 2005.

[5] J. D. Pack, F. Noo, and H. Kudo, "Investigation of saddle trajectories for cardiac CT imaging in cone-beam geometry," *Physics in Medicine and Biology*, vol. 49, no. 11, pp. 2317–2336, 2004.

[6] H. Yang, M. Li, K. Koizumi, and H. Kudo, "View-independent reconstruction algorithms for cone beam CT with general saddle trajectory," *Physics in Medicine and Biology*, vol. 51, no. 15, pp. 3865–3884, 2006.

[7] N. Gindrier, R. Clackdoyle, S. Rit, and L. Desbat, "Cone-beam reconstruction from n-sin trajectories with transversely-truncated projections," in *6th International Conference on Image Formation in X-Ray Computed Tomography*, (Regensburg), pp. 46–49, 2020.

[8] X. Pan, D. Xia, Y. Zou, and L. Yu, "A unified analysis of FBP-based algorithms in helical cone-beam and circular cone- and fan-beam scans," *Physics in Medicine & Biology*, vol. 4349, 2004.

[9] F. Noo, R. Clackdoyle, and J. D. Pack, "A two-step Hilbert transform method for 2D image reconstruction," *Physics in Medicine and Biology*, vol. 49, no. 17, pp. 3903–3923, 2004.

[10] M. Defrise, F. Noo, R. Clackdoyle, and H. Kudo, "Truncated Hilbert transform and image reconstruction from limited tomographic data," *Inverse Problems*, vol. 22, no. 3, pp. 1037–1053, 2006.

[11] S. Rit, M. Vila Oliva, S. Brousmiche, R. Labarbe, D. Sarrut, and G. C. Sharp, "The Reconstruction Toolkit (RTK), an open-source cone-beam CT reconstruction toolkit based on the Insight Toolkit (ITK)," *Journal of Physics: Conference Series*, vol. 489, no. 1, 2014.